Hindawi
Security and Communication Networks
Volume 2022, Article ID 9754748, 1 page
https://doi.org/10.1155/2022/9754748

Retraction

Retracted: Large-Scale Shopping Mall Architectural Design Based on Intelligent BIM Technology

Security and Communication Networks

Received 11 November 2022; Accepted 11 November 2022; Published 22 November 2022

Security and Communication Networks has retracted the article titled "Large-Scale Shopping Mall Architectural Design Based on Intelligent BIM Technology" [1] due to concerns that the peer review process has been compromised.

Following an investigation conducted by the Hindawi Research Integrity team [2], significant concerns were identified with the peer reviewers assigned to this article; the investigation has concluded that the peer review process was compromised. We therefore can no longer trust the peer review process, and the article is being retracted with the agreement of the Chief Editor.

References

[1] Y. Zhou and I. Mishaal, "Large-Scale Shopping Mall Architectural Design Based on Intelligent BIM Technology," *Security and Communication Networks*, vol. 2022, Article ID 3116074, 12 pages, 2022.

[2] L. Ferguson, "Advancing Research Integrity Collaboratively and with Vigour," 2022, https://www.hindawi.com/post/advancing-research-integrity-collaboratively-and-vigour/.

Hindawi
Security and Communication Networks
Volume 2022, Article ID 3116074, 12 pages
https://doi.org/10.1155/2022/3116074

Research Article

Large-Scale Shopping Mall Architectural Design Based on Intelligent BIM Technology

Yuan Zhou[1] **and Ibrahim Mishaal**[2]

[1]*Xi'an University of Architecture and Technology Huaqing College, Xi'an, Shaanxi Province, China*
[2]*Department of Management, Kyrgyz-Turkish Manas University, Bishkek, Kyrgyzstan*

Correspondence should be addressed to Ibrahim Mishaal; dr.ibrahim@email.cu.edu.kg

Received 7 May 2022; Revised 24 May 2022; Accepted 31 May 2022; Published 23 June 2022

Academic Editor: Muhammad Arif

In this paper, limit analysis method and limit analysis finite element method are used to study the stability of large-scale shopping mall building structure. Moreover, this paper combines data analysis to verify the algorithm analysis process of this paper and uses statistical methods to verify that the algorithm proposed in this paper is applicable to the architectural design of large shopping malls. Furthermore, this work uses BIM and finite element technologies to test the usefulness of this strategy by simulating the shopping mall design process. The experimental research shows that the large-scale shopping mall architectural design model proposed in this paper, which is based on intelligent BIM technology, has a good large-scale shopping mall architectural design effect as well as a large-scale shopping mall architectural structure analysis effect.

1. Introduction

The architectural layout, spatial form, and environmental atmosphere of public buildings are constantly changing. Nowadays, public buildings have gradually become the main place for handling business activities and gradually become the basis of social production with the progress of society. In order to meet this development demand, public buildings need to be diversified in form and function. In particular, the rapid development of social informatization in recent years has accelerated the speed of this change. There have been many large-scale multistory public buildings such as comprehensive shopping malls and large supermarkets, such as Carrefour supermarket, Wanda shopping mall, and Wal-Mart supermarket. These buildings are highly comprehensive in terms of function and generally cover underground parking lots, above-ground shopping malls, cinemas, restaurants, etc., and generally require larger column grids, higher stories, and open spaces. Therefore, the choice of the structural system has a greater impact on the cost. In most cases, the structural form of these buildings will choose a reinforced concrete frame structure. Although this structure uses a lot of steel and cement, its cost is higher than that of other hybrid structures. It has the qualities of employing beams and columns to support the weight, with the walls serving solely as a means of separation and enclosure, allowing for more flexibility in the design of rooms, as well as the size and form of doors and windows. The designer may make maximum use of the building's space according to the specifications and readily meet the various needs of the consumers. As a result, reinforced concrete frame structures are often used for multistory and large-story public buildings. The lateral rigidity of the building, however, is poor because of the high story and vast span. In order to achieve the side shift criteria, it is often essential to expand the cross-sectional dimensions of the beam and column, which increases the structure's cost and compromises the use function.

The business environment is mostly related to the market survey of business planning, involving many issues such as economic environment and living structure, urban structure and urban development planning, business development planning and policies, customer consumption behavior, regional retail industry structure and market conditions,

regional competition relationships, the supply of future commercial real estate, and the infrastructure of the area where the business is located [1]. The analysis results of this type of investigation should be given by the project planning document or design task book. The project environment has an important impact on the location of the shopping mall and has a certain impact on the design of the shopping mall. Moreover, architects need to pay attention to the project environment of shopping mall construction [2]. For shopping malls, there is a saying of "one step and three cities," and a small difference in location will result in a loss of performance by thousands of miles. It can be seen that the importance of "situation" in shopping malls is self-evident. The so-called "site force" in the narrow sense refers to the site selection conditions of the shopping mall, and in the broad sense, it refers to the shopping mall project environment. The project environment refers to the collection of various subjective and objective conditions that restrict the existence of shopping malls. It includes the geographic environment of shopping mall site selection, commercial project planning influencing factors on design, various policy norms and constraints of urban planning, and commercial environment of shopping mall operation, traffic environment, and urban context [3].

In order to improve the design effect of large-scale shopping malls, this paper combines BIM technology and finite element analysis algorithms to improve the smart shopping mall design system and uses experimental research to verify the model of this paper, which provides a theoretical reference for subsequent large-scale shopping mall architectural design.

2. Related Work

The frame shear wall construction was improved and compared in the literature [4]. The stiffness ratio between the frame and the shear wall was chosen as the design variable, the least horizontal seismic load was chosen as the objective function, and the maximum interstory angular displacement and the maximum interstory angular displacement were chosen as the design variables. The two characteristics of shear wall stiffness that are not equal to zero are employed as constraints, and a mathematical model for structural optimization is created. The author solves the optimal stiffness ratio by running the program and then uses the calculation formula of the stiffness ratio to convert the stiffness ratio into the number and thickness of the shear walls. The conclusion is that the greater the number of shear walls, the greater the seismic performance of the structure. It will be improved, and each structure has the most appropriate number of shear walls; when general shear walls are arranged in the structure, a certain number of short-leg shear walls are arranged at the same time to make them work together, which is more conducive to the seismic resistance of the structure. Reference [5] conducted an optimization study on the frame shear wall structure under horizontal earthquakes. In the article, the optimal stiffness characteristic interval was discussed, and the optimization model was established to make the structure when the maximum interstory displacement angle meets the specified limit of the code. The effect is minimal, and a set of optimization programs have been written in computer language. Through calculation and analysis of examples, the stiffness of shear wall and building height, structural self-weight, total number of layers of the structure, site characteristic period, maximum horizontal earthquake influence coefficient, and elastic interlayer are calculated and analyzed. The relationship between the displacement angle limit and the period reduction coefficient of nonbearing walls is considered, and the basic natural vibration period of the structure is used to verify the rationality of the calculated number of shear walls. Literature [6] optimized the lateral stiffness of the concrete frame shear wall structure, analyzed how the frame and the shear wall work together, obtained the expressions of internal force and displacement, and proposed a solution for the optimal stiffness of the structure The method of eigenvalue, then derives the expression of the optimal stiffness of the shear wall on the basis of the displacement limit of the structure vertex. The elastoplastic performance of the short-leg shear wall was investigated and researched in the literature [7]. The elastoplastic rod element with a stiff domain mimics the connecting beam of the short-leg shear wall using the equivalent frame method's finite element model. The elastoplastic analysis of the short-leg shear wall is also performed, taking into account the influence of shear deformation. The limb strength coefficient, the integrity coefficient, the flange width, and the reinforcement ratio of the connecting beam, among other factors, are studied throughout the analysis. The impact of these variables on the short-limb shear wall's elastoplastic performance is explored. Literature [8] carried out an experimental study on the seismic performance of reinforced concrete short-leg shear walls, performing low-cycle repeated loading tests on specimens, observing and studying the seismic performance of reinforced concrete short-leg shear walls, and comparing them to ordinary shear walls. Compared. Literature [9] analyzed the parameters of the reinforced concrete frame short-leg shear wall structure, using dynamic and static elastoplastic analysis methods, and it studied the axial compression ratio, the longitudinal reinforcement ratio of the short-leg wall, and the wall under rare earthquakes and the influence of the main section height thickness ratio and other parameters on the seismic performance of the structure is analyzed. It is concluded that increasing the reinforcement ratio of the shear wall will increase the cost, but the seismic capacity of the structure will be significantly increased, and the ductility will also be enhanced; compared with the ordinary shear wall, the height thickness ratio of the short leg shear wall section decreases. If it is reduced, the yield stiffness reduction factor of the structure is increased, and the ductility is better, but the bearing capacity is reduced and the side shift is also increased. Reference [10] conducted a study on the stiffness optimization of reinforced concrete shear wall structure based on seismic response spectrum. The article established a finite element model of a sixteen-story shear wall structure with controlled deformation as a constraint condition, and the thickness of the shear wall was used as a design variable. The light structure as the objective function is taken for optimization. After optimization, the bottom and internal stresses become higher, and

concentrated stress occurs in the corners, the middle roof, and the open shear wall. The seismic effect of the structure and the floor slab with the maximum displacement angle are in the middle of the structure, and whiplash appears on the top of the structure. Tip effect. Literature [11] analyzes the shape control factors of the overall optimization design of the high-rise frame shear wall structure. Starting from the basic theory of structural optimization design and shape control factors, it introduces the characteristics and control of the optimization control factors of the high-rise frame-shear wall structure. Research and analysis show that structural system, building height, building plane aspect ratio, and vertical aspect ratio play an important role in structural optimization. Literature [12] conducted experimental research and numerical analysis on steel plate shear walls with only beam single-plate webs (SSW-BO) and found that using HYS mesh plates in SSW-BO is an effective solution to compensate for low shear capacity and low energy consumption due to separation from the steel plate. In addition, the finite element software ABAQUS has studied the performance of SSW-BO through nonlinear analysis, and the final experimental results are compared with the numerical results, showing good consistency. Literature [13] uses STAAD-Pro software to analyze the three-dimensional model of reinforced concrete frame structure resisting several specific external forces. Through the analysis model, it is found that the shear force of the shear wall starts to affect the shear wall frame and the inner frame at 50% of the building height. The horizontal shear distribution between the two produces a marginal effect, but the building height still plays an important role in the interstory shear distribution.

3. Research on Shopping Mall Building Stability Based on Limit Analysis Method

This paper proposes a new model of shopping mall building stability analysis based on the discrete mechanism ("point generating point" mechanism). Then, based on the upper limit method of limit analysis, this paper proposes an analytical formula for calculating the support force to be sought. After that, this paper compares the results of this section with the previous research results to verify the accuracy of the model proposed in this section. Finally, this article examines and discusses the impact of numerous influencing characteristics (such as geometry and material parameters) on shopping mall stability.

The discrete mechanism is utilised to build the corner failure mechanism in order to investigate the stability of the circular tunnel's face. Since its introduction, the discrete mechanism has been extensively employed to tackle stability issues in a variety of engineering constructions.

This section will first propose a new destruction mechanism based on the discrete mechanism. It can be seen from Figure 1 that $P(i)$ is a point on the lower sliding surface of the newly proposed failure mechanism, θ_i is the angle between the line $OP(i)$ and the straight direction, and $d\theta$ is the angle between the line $OP(i)$ and $OP(i+1)$. When r_A and θ_A are known, the coordinates of the rotation center O can be expressed as follows [14]:

$$\begin{cases} x_o = -r_A \cos\theta_A, \\ y_o = r_A \sin\theta_A. \end{cases} \tag{1}$$

It can be seen from Figure 1 that the key point of the new failure mechanism generation is to solve the failure sliding surface $P(i+1)$ under the premise of the known point $P(i)$ coordinate. Figure 1 shows the process of solving $P(i+1)$ with a known $P(i)$ coordinate.

It can be seen from Figure 2 that $\overrightarrow{v}_i = (x_v, y_{v_v})$ is the unit speed of the point $P(i)$ around the center of rotation O, and $\overrightarrow{n}_i = (x_{n_i}, y_{n_i})$ is the unit normal vector of the microsegment $P(i)P(i+1)$. According to Figure 2, the unit speed of point $P(i)$ can be expressed as follows [15]:

$$\begin{cases} x_{v_i} = -\sin\theta_i, \\ y_{v_i} = \cos\theta_i. \end{cases} \tag{2}$$

According to the Mohr–Coulomb fluidity law, the angle between the unit velocity of point $P(i)$ and the unit normal vector of the microsegment $P(i)P(i+1)$ is $(\pi/2)+\varphi_i$. Therefore, according to the Mohr–Coulomb fluidity rule, the unit normal vector of the microsegment $P(i)P(i+1)$ can be obtained as follows:

$$\begin{cases} x_{n_i} = -\cos(\theta_i + \varphi_i), \\ y_{n_i} = -\sin(\theta_i + \varphi_i). \end{cases} \tag{3}$$

Since $\overrightarrow{n}_i = (x_n, y_n)$ is the unit normal vector of the microsegment $P(i)P(i+1)$, the following relationship can be obtained:

$$\overrightarrow{n_i}\left(\overrightarrow{P_iO} + \overrightarrow{OP}_{i+1}\right) = 0. \tag{4}$$

In order to solve the coordinate of $P(i+1)$, this section will express $OP(i+1)$ as the following form:

$$\overrightarrow{OP}_{i+1} = \lambda_{i+1}\overrightarrow{\delta_{i+1}}. \tag{5}$$

λ_{i+1} indicates the length of $OP(i+1)$ which can be expressed as follows:

$$\lambda_{i+1} = \frac{x_{n_i}(x_0 - x_i) + y_{n_i}(y_0 - y_i)}{x_{n_i}\cos\theta_{i+1} + y_{n_i}\sin\theta_{i+1}}. \tag{6}$$

Combining the above equations, the expression of point $P(i+1)$ can be known as follows:

$$\begin{cases} x_{i+1} = x_0 - \lambda_{i+1}\cos\theta_{i+1}, \\ y_{i+1} = y_0 - \lambda_{i+1}\sin\theta_{i+1}. \end{cases} \tag{7}$$

Substituting formula (6) into formula (7), the $P(i+1)$ expression can be obtained as follows [16]:

$$\begin{cases} x_{i+1} = x_0 - \dfrac{x_{n_i}(x_0 - x_i) + y_{n_i}(y_0 - y_i)}{x_{n_i}\cos\theta_{i+1} + y_{n_i}\sin\theta_{i+1}}\cos\theta_{i+1}, \\ y_{i+1} = y_0 - \dfrac{x_{n_i}(x_0 - x_i) + y_{n_i}(y_0 - y_i)}{x_{n_i}\cos\theta_{i+1} + y_{n_i}\sin\theta_{i+1}}\sin\theta_{i+1}. \end{cases} \tag{8}$$

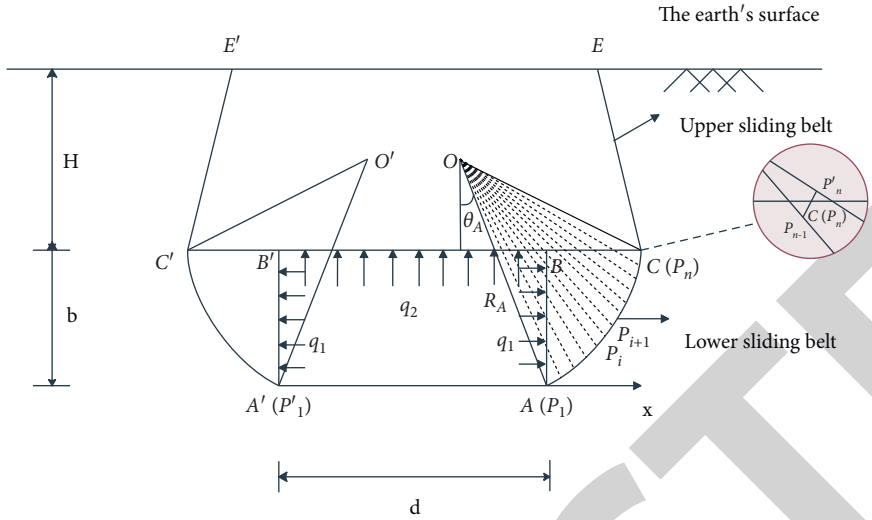

Figure 1: Schematic diagram of the new destruction mechanism.

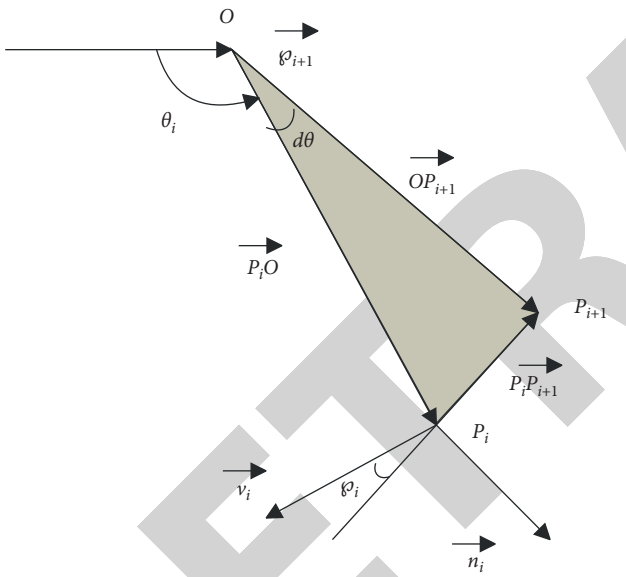

Figure 2: Schematic diagram of generating point P(i+1) from point P(i).

It can be seen from Figure 2 that when the generated point $P(i+1)$ exceeds the line AC, the coordinates of point C of the mall building destruction mechanism generated by the discrete mechanism can be obtained according to the linear calculation method, and the expression is as follows:

$$\begin{cases} x_C = x_n - \dfrac{(y_n - d)(x_n - x_{n-1})}{y_n - y_{n-1}}, \\ y_C = b. \end{cases} \tag{9}$$

The failure planes CE and CE are assumed to be lines with an angle φ_0 from the vertical direction (see Figure 1). It can be seen from formulas (1) and (9) that when the geometric parameters r_A and θ_A are known, a new failure mode of shopping mall buildings can be obtained.

The ultimate sustaining force of shopping malls may be addressed using the virtual work concept of the upper limit technique of limit analysis when the discrete mechanism is utilised to develop new failure modes for shopping malls. The final support force of the mall structure may be calculated using the relationship between total internal power and total dissipated power acting on the slip surface. It can be seen from Figure 1 that the external forces acting on the failure mode of a shopping mall building include supporting forces $q1$ and $q2$ (Figure 1), soil gravity in the failure mode, and ground load. The solution process is as follows [17].

3.1. Internal Power

3.1.1. Supporting Force q1 and q2 Power. The power of supporting force q1 can be solved as follows:

$$W_{q_1} = \iint_{\Sigma} q_1 \cdot v \, d\sum = \frac{1}{2}\omega q_1 \cdot r_A^2 \left[\left(\frac{\cos\theta_A}{\cos\theta_B}\right)^2 - 1\right]. \tag{10}$$

The power of supporting force q2 can be expressed as follows:

$$W_{q_2} = -q_2 b v_0. \tag{11}$$

Here, v_0 represents the speed of the broken block $CC'E'E$ (due to the symmetry of the broken block $CC'E'E$, it can be known that the direction of the broken block's speed is straight downward).

Therefore, the total power of the available supporting forces q_1 and q_2 is [18]

$$W_q = -q_2 b v_0 + \frac{1}{2}\omega q_1 r_A^2 \left[\left(\frac{\cos\theta_A}{\cos\theta_B}\right)^2 - 1\right]. \tag{12}$$

We assume $q_1 = Kq_2$, and equation (12) is expressed as the following form:

$$W_q = -q_2 b v_0 + \frac{K}{2}\omega q_2 r_A^2\left[\left(\frac{\cos\theta_A}{\cos\theta_B}\right)^2 - 1\right]. \quad (13)$$

In this section, when analyzing the stability of shopping malls, we only consider the case of $K = 1$.

3.1.2. Power per Soil Weight. The power of some unit soil weight under the new damage mechanism constructed in this section can be expressed as follows:

$$W_{\gamma 1} = \iiint_V \vec{\gamma}\cdot\vec{v}\,dV = \omega\sum_{i=1}^{n}\gamma R_i S_i\cos\theta_i. \quad (14)$$

Among them, there are

$$R_i = \sqrt{\left(\frac{x_B + x_i + x_{i+1}}{3} - x_o\right)^2 + \left(\frac{y_B + y_i + y_{i+1}}{3} - y_o\right)^2}, \quad (15)$$

$$S_i = \frac{1}{2}\cdot\left(x_B y_i - x_i y_B + x_i y_{i+1} - x_{i+1} y_i + x_{i+1} y_B - x_B y_{i+1}\right). \quad (16)$$

The power of part of the unit soil weight on the new damage mechanism constructed in this section can be expressed as follows:

$$W_{\gamma 2} = \frac{1}{2}\gamma S_{CCEE} v_0. \quad (17)$$

Here, v_0 represents the speed of the broken block $CC'E'E$ (due to the symmetry of the broken block $CC'E'E$, it can be known that the direction of the speed of the broken block is straight downward).

Combining formula (14) and (17), the power per unit weight of the soil in the final damage mechanism can be expressed as follows:

$$W_\gamma = \omega\sum_{i=1}^{n}\gamma R_i S_i\cos\theta_i + \frac{1}{2}\gamma S_{CCEE} v_0. \quad (18)$$

3.2. Power Dissipation. It can be seen from Figure 2 that the total power dissipation along the slip surface includes the power dissipation along the slip surface AC (or $A'C'$) and the power dissipation along the slip surface CE (or $C'E'$). Among them, the power dissipation along the slip surface AC is

$$W_{D1} = \iint_S c\vec{v}\cos\varphi dS = \omega\sum_{i=1}^{n} c_i\cdot\cos\varphi_i\cdot R_i\cdot S_i. \quad (19)$$

Among them, there are

$$R_i = \sqrt{\left(\frac{x_i + x_{i+1}}{2} - x_0\right)^2 + \left(\frac{y_i + y_{i+1}}{2} - y_0\right)^2},$$
$$S_i = \sqrt{\left(\frac{x_i - x_{i+1}}{2}\right)^2 + \left(\frac{y_i - y_{i+1}}{2}\right)^2}. \quad (20)$$

The power dissipation along the slip surface CE can be expressed as follows [19]:

$$W_{D2} = c_{CE/2} v_0 L_{CE}\cos\varphi_{CE/2}. \quad (21)$$

Here, $c_{CE/2}$ represents the cohesive force in the middle of the slip surface CE, $\varphi_{CE/2}$ represents the friction angle in the middle of the slip surface CE, L_{CE} represents the length of the slip surface CE, and v_0 represents the speed of the broken block $CC'E'E$ (due to the symmetry of the broken block $CC'E'E$, it can be seen that the speed direction of the broken block is straight downward).

The total power dissipation can be calculated by equations (19) and (21).

Finally, the ultimate supporting force on the surrounding rock of the mall building can be solved as follows:

$$W_c = W_\gamma + W_{q_1} + W_{q_2}. \quad (22)$$

This section discusses the influence of heterogeneous geotechnical parameters on the stability of surrounding rocks of shopping mall buildings. Figure 3 shows the schematic diagram of the ultimate supporting force q ($q1 = q2$) with the variation of the heterogeneous friction angle. Figure 3 shows how the final sustaining force decreases as the ground friction angle increases. When the ground friction angle is considerable, the final sustaining force drops practically linearly as the ground friction angle increases. In addition, it can be seen from Figure 3 that as the heterogeneity coefficient λ_φ increases, the ultimate supporting force value also gradually decreases. Moreover, when the ground friction angle is small, the limit supporting force changes more obviously with the increase of the heterogeneity coefficient λ_φ. The above discussion shows that the nonhomogeneous friction angle coefficient has a non-negligible influence on the ultimate supporting force, and ignoring the influence of the heterogeneous friction angle coefficient λ_φ on the ultimate supporting force will result in inaccurate results. Therefore, considering the heterogeneous friction angle can better assess the stability of shopping malls [20].

The impact of heterogeneous rock-soil cohesion on the stability of surrounding rock of shopping mall structures is discussed in this section. Figure 4 depicts the change in the limit sustaining force q as a function of the heterogeneous cohesive force. Figure 4 shows that when the ground cohesiveness increases, the final sustaining force reduces linearly. Figure 4 clearly shows that when the heterogeneity coefficient c increases, the limit support force value lowers. The preceding explanation demonstrates that the coefficient of heterogeneous cohesion c has a significant impact on the eventual sustaining force, and that disregarding this influence would result in erroneous findings. Therefore, considering the heterogeneous cohesion can better evaluate the stability of shopping malls [21].

The double helix failure mechanism is used to study the stability of the face of a circular tunnel. Since the double helix mechanism was proposed, this method has been widely used to solve many stability problems of engineering structures (the stability of tunnels and slopes).

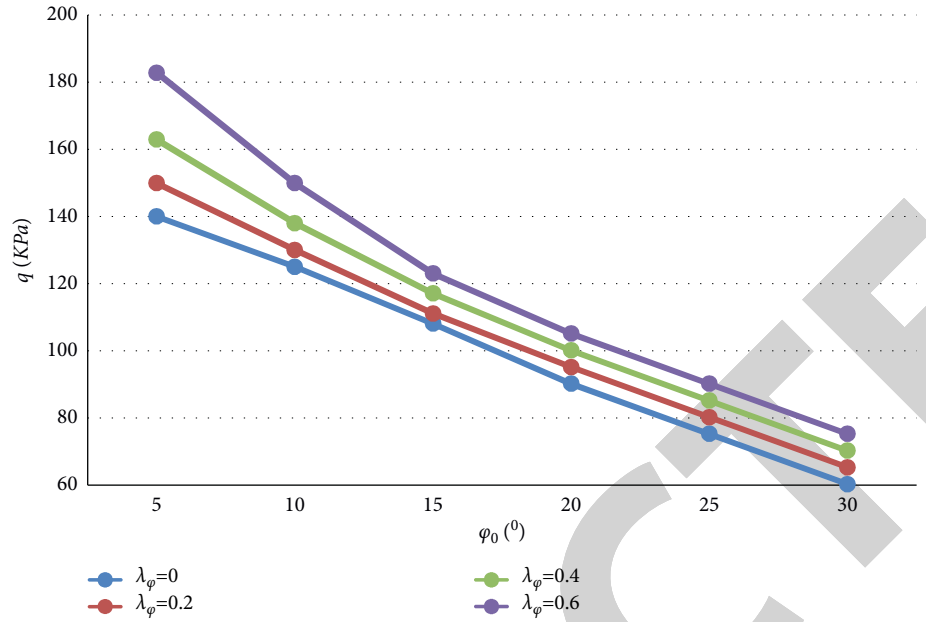

Figure 3: The influence of the heterogeneous internal friction angle on the ultimate supporting force q.

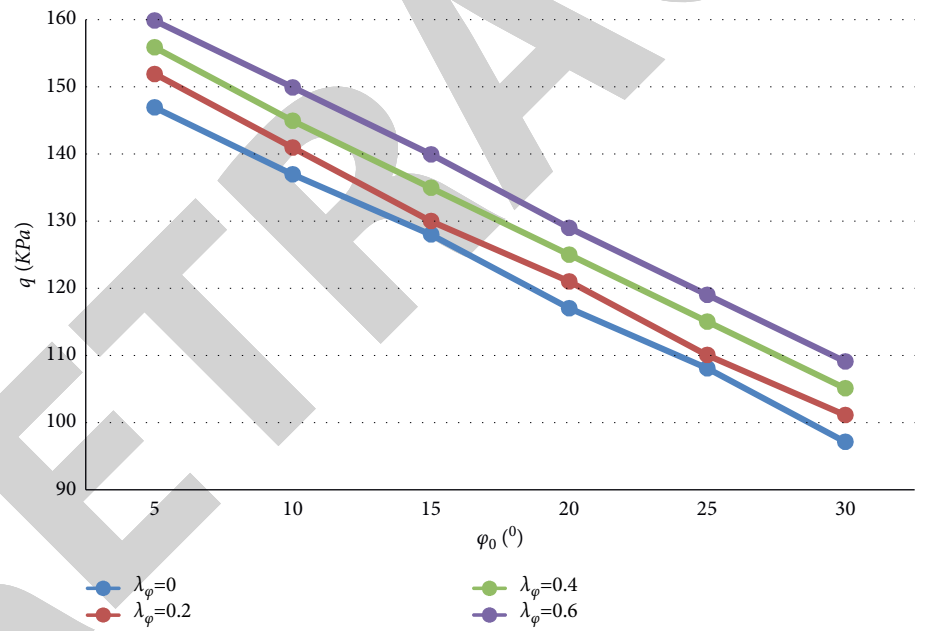

Figure 4: The influence of heterogeneous cohesion on the ultimate supporting force q.

Figure 5 shows the traditional double helix damage mechanism. The expression of the traditional double helix damage mechanism can be expressed as follows:

$$\begin{cases} AC: r = r_A e^{(\theta - \theta_A)\tan\varphi}, \\ B\ D: r = r_B e^{(\theta_B - \theta)\tan\varphi}. \end{cases} \tag{23}$$

This mechanism can be used to evaluate the stability of the excavation surface of the low space of a shopping mall building under the condition of homogeneous soil (with and without considering seepage) and to solve the ultimate support pressure acting on the excavation surface. This damage mechanism, however, cannot be employed to investigate the impact of heterogeneous soil on the excavation surface of a retail mall's low-level area. As a result, the classic double helix failure mechanism has a limited utility in geotechnical engineering. This section suggests an enhanced new active destruction process based on the "point spawning point" technique as a result of this (Figure 6). It can be seen from Figure 6 that the focus of the new failure mechanism generat"on is to solve the fa"lure sliding surface $P(i+1)$ (or $P'(i+1)$) under the premise of the known coordinates of the point $P(i)$ (or $P'(i)$). Based on the traditional double helix failure model and the "point generation" mechanism, based

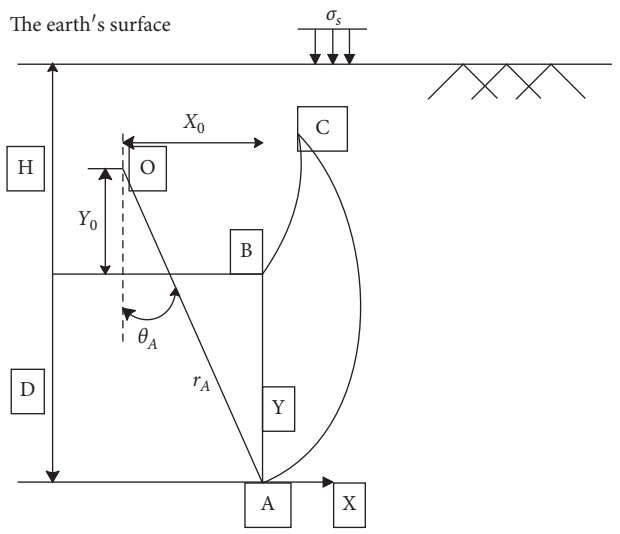

Figure 5: Traditional double helix destruction mechanism.

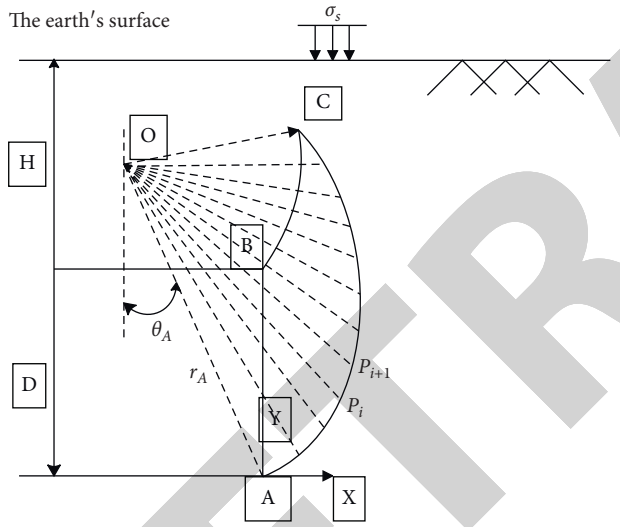

Figure 6: Destruction mechanism based on "point spawning point."

on the known coordinates of point $P(i)$ (or $P'(i+1)$), the expression process for solving the failure sliding surface $P(i+1)$ (or $P'(i+1)$) is proposed as follows.

First, when r_A and θ_A are known, the coordinates of the rotation center O point can be expressed as follows:

$$\begin{cases} x_o = -r_A \cos\theta_A, \\ y_o = r_A \sin\theta_A. \end{cases} \tag{24}$$

According to the double helix formula and the value of the angle $d\theta$ between the line $P(i)O$ (or $(P'(i)O)$) and the line $P(i+1)O$ (or $P'(i+1)O$), the distance r_{i+1} (or r_{i+1}') between point $P(i+1)$ (or $P'(i)$) and point O can be obtained, and the expression can be solved as follows [22]:

$$\begin{cases} AC\text{: } r_{i+1} = r_i e^{(\theta_{i+1}-\theta_i)\tan\varphi_i}, \\ B\ D\text{: } r_{i+1}' = r_i' e^{(\theta_i-\theta_{i+1}')\tan\varphi_i}. \end{cases} \tag{25}$$

According to the value of the distance r_{i+1} (or r_{i+1}') between point $P(i+1)$ (or $P'(i+1)$) and point O and the angle θ_{i+1} (or θ_{i+1}') between line $P(i+1)O$ (or line $P'(i+1)O$) and the straight direction, the coordinate expression of the point $P(i+1)$ (or $P'(i+1)$) can be obtained as follows:

$$\begin{cases} x_{i+1} = r_{i+1}\sin\theta_{i+1} + x_o, \\ y_{i+1} = r_{i+1}\cos\theta_{i+1}. \end{cases} \tag{26}$$

Alternatively, it is

$$\begin{cases} x_{i+1}' = r_{i+1}'\sin\theta_{i+1}' + x_o, \\ y_{i+1}' = r_{i+1}'\cos\theta_{i+1}'. \end{cases} \tag{27}$$

In addition, the coordinates of point C can be obtained by combining equations (23) to (27). It is worth noting that when $i=1$, $r_i = r_A, \in r_i' = r_B, \theta_i = \theta_A$ and $\theta_i' = \theta_B'$. The algorithm uses straight lines to connect the obtained points in sequence to obtain the constructed new active destruction mechanism.

When the new failure mode of the excavation surface of the low space of the shopping mall building is generated, according to the virtual work principle of the limit analysis upper limit method, the limit support force acting on the excavation surface of the low space of the shopping mall building can be solved. The connection between the total internal force power and the total dissipation power operating on the slip surface may be used to calculate the final sustaining force acting on the excavation surface of the low space of a shopping mall construction. Supporting force q, soil gravity in the failure model, and ground load are examples of external forces acting on the failure mode of the excavation surface in subterranean space. The solution process is as follows.

3.3. Solving Internal Force Power

3.3.1. Supporting Force q Power. The power of the supporting force q acting on the excavation surface of the low space of the shopping mall building can be solved as follows:

$$W_q = \iint_\Sigma q \cdot v\mathrm{d}\sum = \frac{1}{2}\omega q \cdot r_A^2\left[\left(\frac{\cos\theta_A}{\cos\theta_B}\right)^2 - 1\right]. \tag{28}$$

3.3.2. Upper Heavy γ Power. The damage mechanism is divided horizontally to find the power per unit soil weight γ. The power per unit soil weight of the new damage mechanism constructed in this section can be expressed as follows:

$$W_\gamma = \iiint_V \vec{\gamma}\cdot\vec{v}\,\mathrm{d}V = \omega\sum_{i=1}^{n}\gamma R_i S_i\cos\theta_i. \tag{29}$$

Here, R_i represents the distance from the center of gravity of each i-th horizontal bar to point O, and S_i represents the area of each i-th horizontal bar.

In addition, based on assumptions, this section does not consider the impact of ground load on the ultimate support pressure during the analysis of the stability of the excavation surface in the low space of the shopping mall building. Therefore, this section will not discuss the influence of ground load on the ultimate supporting force acting on the excavation surface of the low space of the shopping mall building.

3.4. Solving the Total Power Dissipation. The dissipated power is the power generated by the cohesive force along the failure mode slip surface. It can be seen from Figure 6 that the total dissipated power includes the power dissipated along AC and along BC, and the expressions are as follows:

Among them, the power dissipation along the slip surface AC is

$$W_{D1} = \iint_S c\overrightarrow{v}\cos\varphi \mathrm{d}S = \omega \sum_{i=1}^{n} c_i \cdot \cos\varphi_i \cdot R_i \cdot L_i. \tag{30}$$

Among them, there are

$$R_i = \sqrt{\left(\frac{x_i + x_{i+1}}{2} - x_0\right)^2 + \left(\frac{y_i + y_{i+1}}{2} - y_0\right)^2}, \qquad L_i = \sqrt{(x_i - x_{i+1})^2 + (y_i - y_{i+1})^2}. \tag{31}$$

Among them, the power dissipation along the slip surface *BC* is

$$W_{D2} = \iint_S c\overrightarrow{v}\cos\varphi \mathrm{d}S = \omega \sum_{i=1}^{n} c_i \cdot \cos\varphi_i \cdot R_i' \cdot L_i'. \tag{32}$$

Among them, there are

$$R_i' = \sqrt{\left(\frac{x_i' + x_{i+1}'}{2} - x_0\right)^2 + \left(\frac{y_i' + y_{i+1}'}{2} - y_0\right)^2}, \tag{33}$$

$$L_i' = \sqrt{(x_i' - x_{i+1}')^2 + (y_i' - y_{i+1}')^2}. \tag{34}$$

Therefore, the total power dissipation can be expressed as the following form:

$$W_D = \omega \sum_{i=1}^{n} c_i \cdot \cos\varphi_i \cdot R_i \cdot L_i + \omega \sum_{i=1}^{n} c_i \cdot \cos\varphi_i \cdot R_i' \cdot L_i'. \tag{35}$$

3.5. Solving the Ultimate Supporting Force. According to the upper limit method of limit analysis, it can be known that the total power of internal force is equal to the total power of dissipation. Combining equations (28) to (35), the expression of the ultimate supporting force of the excavation surface in the low space of the shopping mall building can be obtained as follows:

$$q = \frac{\omega \sum_{i=1}^{n} \gamma R_i S_i \cos\theta_i - \omega \sum_{i=1}^{n} c_i \cdot \cos\varphi_i \cdot R_i \cdot L_i + \omega \sum_{i=1}^{n} c_i \cdot \cos\varphi_i \cdot R_i' \cdot L_i'}{(1/2)\omega r_A^2 \left[\left(\cos\theta_A / \cos\theta_B\right)^2 - 1\right]}. \tag{36}$$

This section discusses the influence of heterogeneous rock and soil parameters on the stability of surrounding rock in square underground spaces. Figure 7 shows a schematic diagram of the change of $(q/\gamma\ D)$ with the heterogeneous friction angle. It can be seen from Figure 7 that as the ground friction angle increases, $(q/\gamma\ D)$ gradually decreases. When the ground friction angle is larger, $(q/\gamma\ D)$ changes smaller and smaller with the increase of the ground friction angle. In addition, it can be seen from Figure 7 that as the heterogeneity coefficient λ_φ increases, the rate at which $(q/\gamma\ D)$ decreases gradually decreases. However, when the ground friction angle is small, $(q/\gamma\ D)$ changes significantly with the increase of the heterogeneity coefficient λ_φ. The foregoing explanation demonstrates that the nonhomogeneous friction angle coefficient has a significant impact on the eventual supporting force, and that disregarding this impact would result in erroneous findings. Therefore, considering the heterogeneous friction angle can better evaluate the stability of shopping malls.

Figure 8 shows a schematic diagram of $(q/\gamma\ D)$ changing with heterogeneous cohesion. It can be seen from Figure 8 that as the ground friction angle increases, $(q/\gamma\ D)$ decreases linearly. In addition, it can be seen from Figure 8 that as the heterogeneity coefficient λ_c increases, $(q/\gamma\ D)$ also gradually decreases. The above discussion shows that the nonhomogeneous friction angle coefficient has a non-negligible influence on the ultimate supporting force, and ignoring the influence of the heterogeneous cohesion coefficient λ_c on the ultimate supporting force will result in inaccurate results. Therefore, considering the heterogeneous cohesion can better evaluate the stability of shopping malls.

4. Large-Scale Shopping Mall Architectural Design Based on Intelligent BIM Technology

In the initial stage of BIM application, the design process has not changed much, and the division of scheme design stage, preliminary design stage, and construction drawing design stage is still very clear. Some firms, however, have started to concentrate on professional cooperation in each design step in order to better use the synergy of BIM. Figure 9 depicts a typical design process in the early stages of BIM. The present use of BIM is still sensitive to the level of connected software and hardware, which is a significant justification for adopting this method. Simply told, most BIM software today has extremely high computer setup requirements, and even "top configuration" systems cannot handle a large project. As a result, in this situation, the designer would first establish

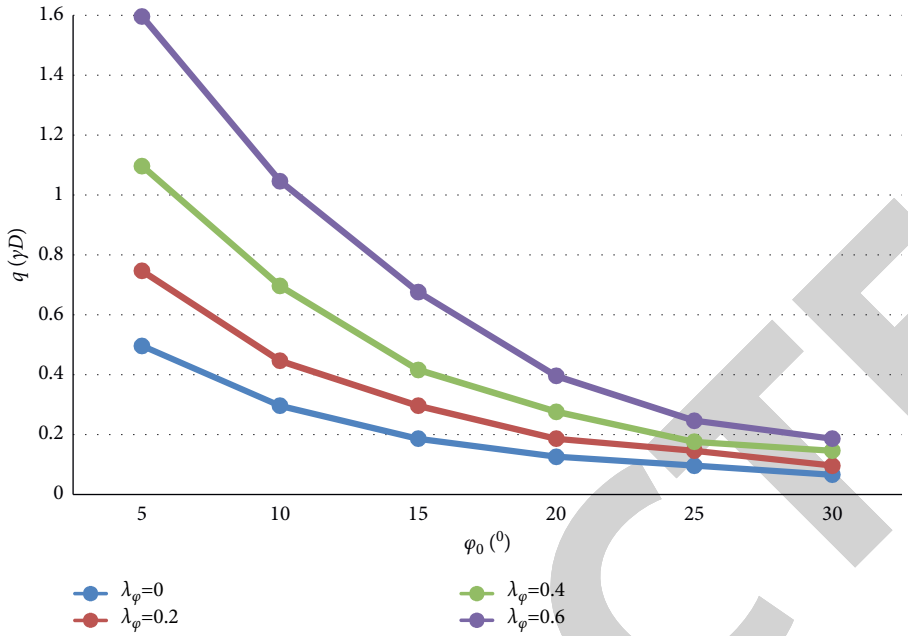

Figure 7: The influence of heterogeneous internal friction angle on the stability of excavated surface.

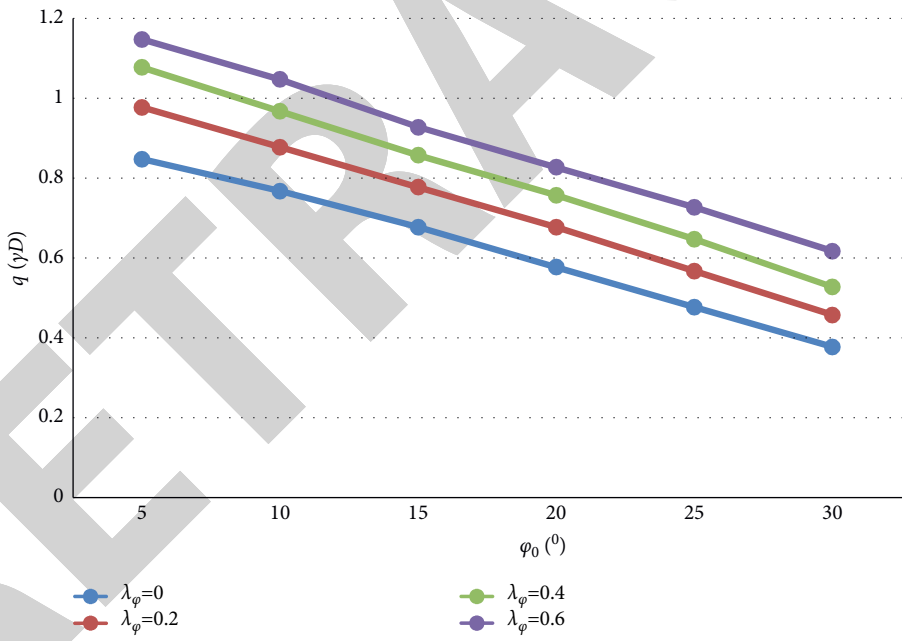

Figure 8: The influence of heterogeneous cohesion on the stability of excavated face.

a design concept (such as managing the project origin coordinates), then model various professions independently, with certain large-scale projects requiring modelling within the same profession. At complex design nodes or key time points, the designer uses the "Link" mode to integrate the design results or export the design results to a special software (such as Autodesk Navisworks) for collaborative work. When one stage of collaborative work is successfully completed, the designer enters the next stage of design work.

This article combines BIM technology and finite element technology and takes a shopping mall as an example to study the effectiveness of this method by simulating the design process of the shopping mall. Figure 10 shows the finite element model of the simulated shopping mall in this paper.

First of all, this paper verifies the effect of the system design proposed in this paper, combines BIM to conduct a comprehensive evaluation of the process of large-scale shopping mall architectural design, and obtains the results shown in Table 1.

The large-scale shopping mall architectural design model based on intelligent BIM technology suggested in this research has an excellent shopping mall architectural design impact, as shown by the aforementioned statistics. The influence of structural finite element analysis of a major

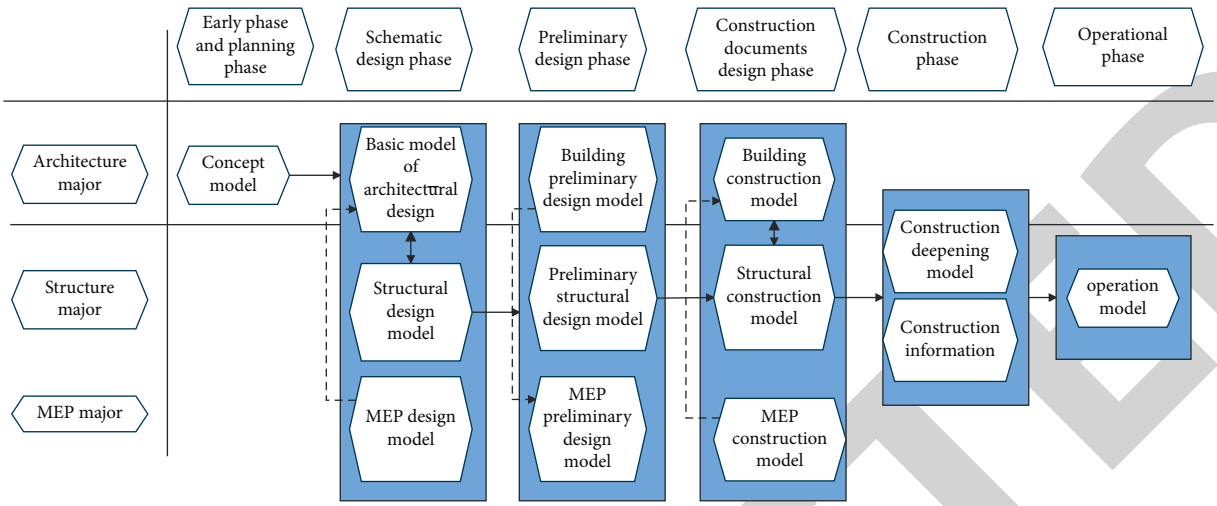

Figure 9: BIM design process at the initial stage.

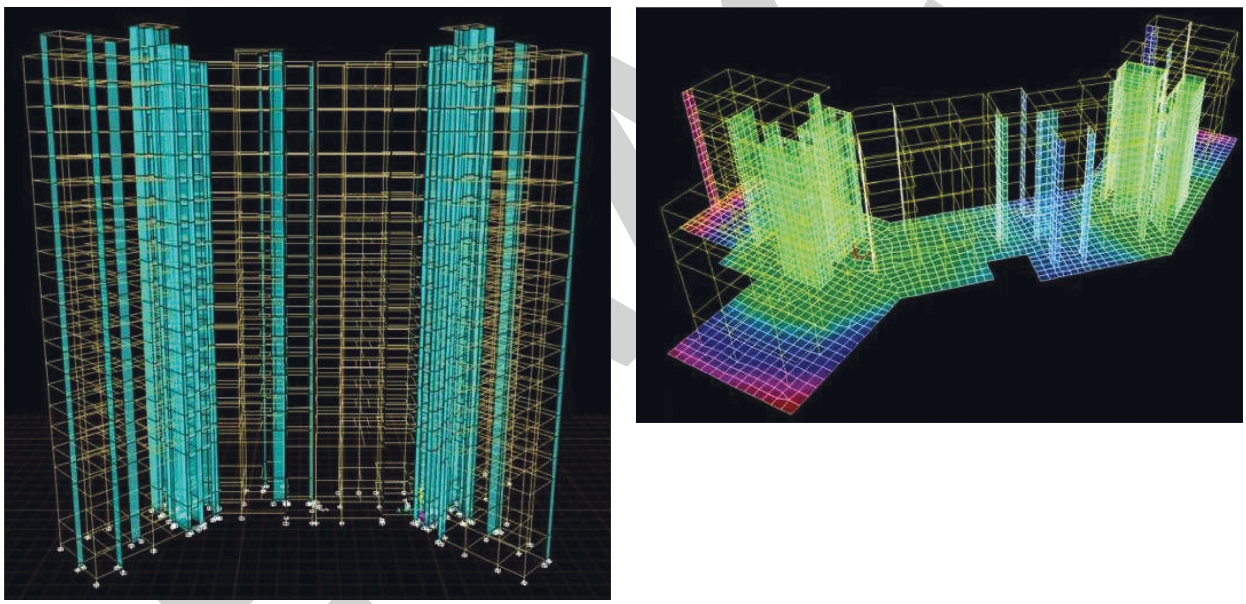

(a) (b)

Figure 10: Finite element analysis model of shopping mall building. (a) Partial finite element analysis of shopping mall buildings. (b) Finite element analysis of the overall structure of shopping malls.

Table 1: Evaluation of shopping mall architectural design effect based on BIM intelligent technology of large-scale shopping mall architectural design model.

Num	Architectural design evaluation
1	80.5559
2	75.8143
3	75.3830
4	71.5944
5	68.9272
6	68.6747
7	81.7511
8	69.0331
9	79.1785
10	81.7189
11	79.8903
12	76.3514
13	82.9396
14	69.9193
15	81.9486
16	70.9332
17	76.7322
18	73.7702
19	73.6390
20	79.7620
21	76.2087
22	71.1080
23	73.6415
24	80.2592
25	74.0047
26	70.9110
27	76.4545
28	68.2340
29	81.6982
30	69.4610
31	82.6639
32	70.3344
33	69.0561
34	74.2149
35	72.9094
36	81.2314
37	72.8330
38	80.9099
39	80.8039
40	71.4435
41	72.7555
42	82.1990
43	79.8660
44	68.7986
45	79.2538

Table 2: Evaluation of the structural analysis effect of the large-scale shopping mall architectural design model based on BIM intelligent technology.

Num	Building structure analysis
1	90.7270
2	84.6731
3	86.0295
4	86.9265
5	71.6231
6	88.6527
7	80.4022
8	87.3672
9	75.4974
10	89.7134
11	77.2815
12	75.6310
13	81.4506
14	76.0609
15	78.3692
16	71.4706
17	89.1021
18	74.2504
19	85.3857
20	89.6187
21	72.6808
22	80.4343
23	87.2656
24	80.4550
25	80.6829
26	74.6498
27	80.9686
28	73.0932
29	86.7402
30	86.7981
31	73.8838
32	72.3059
33	90.7192
34	90.3769
35	88.4537
36	86.5650
37	70.3648
38	80.5353
39	82.8677
40	90.8998
41	88.7535
42	84.4882
43	81.6500
44	82.6974
45	74.4918

shopping mall architectural design model is assessed on this basis, and the findings indicated in Table 2 are achieved.

From the above analysis, it can be seen that the large-scale shopping mall architectural design model based on intelligent BIM technology proposed in this paper has a good shopping mall architectural structure analysis effect.

5. Conclusion

Before proceeding with the architectural design of a large shopping mall, a detailed investigation and analysis of the project environment is required. Moreover, it is necessary to confirm the feasibility of shopping mall construction based

on the analysis results, clarify the business format and construction scale, and determine the direction of the design ideas. Due to the limited time for commercial operation and design, specific projects need to be used selectively in light of actual conditions. However, owing to the challenging inquiry settings, collecting numerous variables may be problematic. As a result, doing qualitative research on shopping malls using just one approach is unscientific. In any chosen study strategy, both qualitative and quantitative research must be employed extensively. This study employs experimental research to validate the model of this paper, which offers a theoretical reference for later large-scale shopping mall architectural design and integrates BIM technology and finite element analysis techniques to enhance the smart shopping mall design system. Through experimental research, it can be seen that the large-scale shopping mall architectural design model based on intelligent BIM technology proposed in this paper has a good large-scale shopping mall architectural design effect and a good large-scale shopping mall architectural structure analysis effect.

Data Availability

The data used to support the findings of this study are included within the article.

Conflicts of Interest

The authors declare that they have no conflicts of interest.

References

[1] R. R. Dong, "The application of BIM technology in building construction quality management and talent training," *Eurasia Journal of Mathematics, Science and Technology Education*, vol. 13, no. 7, pp. 4311–4317, 2017.

[2] X. Qin, Y. Shi, K. Lyu, and Y. Mo, "Using a TAM-TOE model to explore factors of Building Information Modelling (BIM) adoption in the construction industry," *Journal of Civil Engineering and Management*, vol. 26, no. 3, pp. 259–277, 2020.

[3] Y.-C. Kim, W.-H. Hong, J.-W. Park, and G.-W. Cha, "An estimation framework for building information modeling (BIM)-based demolition waste by type," *Waste Management & Research: The Journal for a Sustainable Circular Economy*, vol. 35, no. 12, pp. 1285–1295, 2017.

[4] M. N. Kocakaya, E. Namlı, and Ü. Işıkdağ, "Building information management (BIM), a new approach to project management," *Journal of sustainable construction materials and technologies*, vol. 4, no. 1, pp. 323–332, 2019.

[5] A. Okakpu, A. GhaffarianHoseini, J. Tookey, J. Haar, A. Ghaffarianhoseini, and A. Rehman, "A proposed framework to investigate effective BIM adoption for refurbishment of building projects," *Architectural Science Review*, vol. 61, no. 6, pp. 467–479, 2018.

[6] L. Ustinovičius, A. Puzinas, J. Starynina, M. Vaišnoras, O. Černiavskaja, and R. Kontrimovičius, "Challenges of BIM technology application in project planning," *Engineering Management in Production and Services*, vol. 10, no. 2, pp. 15–28, 2018.

[7] M. O. Fadeyi, "The role of building information modeling (BIM) in delivering the sustainable building value," *International Journal of Sustainable Built Environment*, vol. 6, no. 2, pp. 711–722, 2017.

[8] T. Mandičák, P. Mesároš, and M. Tkáč, "Impact of management decisions based on managerial competencies and skills developed trough BIM technology on performance of construction enterprises," *Pollack Periodica*, vol. 13, no. 3, pp. 131–140, 2018.

[9] L. Ustinovichius, V. Popov, J. Cepurnaite, T. Vilutienė, M. Samofalov, and C. Miedziałowski, "BIM-based process management model for building design and refurbishment," *Archives of Civil and Mechanical Engineering*, vol. 18, no. 4, pp. 1136–1149, 2018.

[10] T. Wei and Y. Chen, "Green building design based on BIM and value engineering," *Journal of Ambient Intelligence and Humanized Computing*, vol. 11, no. 9, pp. 3699–3706, 2020.

[11] S. M. Noor, S. R. Junaidi, and M. K. A. Ramly, "Adoption of building information modelling (bim): factors contribution and benefits," *Journal of Information System and Technology Management*, vol. 3, no. 10, pp. 47–63, 2018.

[12] E. Papadonikolaki, C. van Oel, and M. Kagioglou, "Organising and managing boundaries: a structurational view of collaboration with building information modelling (BIM)," *International Journal of Project Management*, vol. 37, no. 3, pp. 378–394, 2019.

[13] Y. Y. Al-Ashmori, I. Othman, Y. Rahmawati et al., "BIM benefits and its influence on the BIM implementation in Malaysia," *Ain Shams Engineering Journal*, vol. 11, no. 4, pp. 1013–1019, 2020.

[14] A. Koutamanis, J. Heuer, and K. D. Könings, "A visual information tool for user participation during the lifecycle of school building design: BIM," *European Journal of Education*, vol. 52, no. 3, pp. 295–305, 2017.

[15] J. Xu, B. K. Li, and S. M. Luo, "Practice and exploration on teaching reform of engineering project management course in universities based on BIM simulation technology," *Eurasia Journal of Mathematics, Science and Technology Education*, vol. 14, no. 5, pp. 1827–1835, 2018.

[16] C.-J. Chen, S.-y. Chen, S.-h. Li, and H.-t. Chiu, "Green BIM-based building energy performance analysis," *Computer-Aided Design and Applications*, vol. 14, no. 5, pp. 650–660, 2017.

[17] H. R. Abed, W. A. Hatem, and N. A. Jasim, "Adopting BIM technology in fall prevention plans," *Civil Engineering Journal*, vol. 5, no. 10, pp. 2270–2281, 2019.

[18] L. Joblot, T. Paviot, D. Deneux, and S. Lamouri, "Literature review of Building Information Modeling (BIM) intended for the purpose of renovation projects," *IFAC-PapersOnLine*, vol. 50, no. 1, pp. 10518–10525, 2017.

[19] P. Wu, R. Jin, Y. Xu, F. Lin, Y. Dong, and Z. Pan, "The analysis of barriers to bim implementation for industrialized building construction: a China study," *Journal of Civil Engineering and Management*, vol. 27, no. 1, pp. 1–13, 2021.

[20] I. Kim, J. Choi, E. A. L. Teo, and H. Sun, "Development of K-BIM e-Submission prototypical system for the openBIM-based building permit framework," *Journal of Civil Engineering and Management*, vol. 26, no. 8, pp. 744–756, 2020.

[21] A. Dainty, R. Leiringer, S. Fernie, and C. Harty, "BIM and the small construction firm: a critical perspective," *Building Research & Information*, vol. 45, no. 6, pp. 696–709, 2017.

[22] A. Ahankoob, K. Manley, C. Hon, and R. Drogemuller, "The impact of building information modelling (BIM) maturity and experience on contractor absorptive capacity," *Architectural Engineering and Design Management*, vol. 14, no. 5, pp. 363–380, 2018.